

Early X-ray/UV Line Signatures of GRB Progenitors and Hypernovae

C. Weth^{1,2}, P. Mészáros^{1,3,4}, T. Kallman⁵ & M.J. Rees⁶

¹Dpt. of Astronomy & Astrophysics, Pennsylvania State University, University Park, PA 16803

²Inst. f. Astron. & Astrophysik, Univ. Tübingen, a.d. Morgenstelle 10, 72076 Tübingen, Germany

³Institute for Theoretical Physics, University of California, Santa Barbara, CA 93106-4030

⁴Astronomy Dpt., California Institute of Technology, MS 105-24, Pasadena, CA 91125

⁵Code 662, Lab. for High Energy Astrophysics, NASA/Goddard, Greenbelt, MD 20771

⁶Institute of Astronomy, University of Cambridge, Madingley Road, Cambridge CB3 0HA, U.K.

ABSTRACT

We calculate the X-ray/UV spectral line signatures expected from the interaction of a gamma-ray burst afterglow and a dense pre-burst environment produced by the progenitor. We explore the conditions under which Fe line and edge equivalent widths of ~ 1 keV can arise, and discuss the possibility of gaining information about possible progenitor scenarios using X-ray metal line spectra in the first few days of a burst. A wind or supernova shell around the burst produces an X-ray absorption line spectrum and later emission lines, while a hypernova funnel model produces mainly emission lines. The Fe K-edge can in some cases be more prominent than the Fe K- α line. Under simple assumptions for the input continuum luminosity, current reports of observed Fe line luminosities are compatible with an Fe-enriched funnel model, while lower values are expected in shell models.

Subject headings: Gamma-rays: bursts – X-rays: general – Ultraviolet: general – Stars: mass loss – Stars: supernovae: general – Cosmology: miscellaneous

1. Introduction

The nature of the progenitors of gamma-ray bursts (GRB) is an unsettled issue of extreme interest, e.g. Fryer, Woosley & Hartmann 1999, Paczyński 1998, Mészáros, 1998. It is becoming increasingly apparent that whatever the progenitor, a black hole plus debris torus may result which powers the GRB, but the burning question is what gives rise to this system. Both compact binary (NS-NS or BH-NS) mergers, other mergers (WD-BH, He-BH) or the collapse of a massive, fast

rotating star (referred to as hypernovae or collapsars) could lead to such a BH plus debris torus energy source, and much current work centers on discriminating between the various progenitors.

Evidence concerning the progenitor comes both from the accumulating statistics on the off-sets between GRB afterglow optical transients and their host galaxies (Bloom *et al.*1998) and from light curve fits and continuum spectral information providing evidence for either low (Wijers & Galama 1999) or high (Owen *et al.*1998) density in front of the afterglow. However, the most direct diagnostics for the environment are probably X-ray and UV spectral lines (Bisnovatyi-Kogan & Timokhin 1997, Perna & Loeb 1998, Mészáros & Rees 1998b, Böttcher *et al.*1998) and an interesting possible diagnostic for hypernovae or collapsars is the presence of Fe K- α emission lines, produced by fluorescent scattering from the outer parts of the stellar progenitor of the continuum X-ray photons originating in the afterglow of the GRB (Mészáros & Rees 1998b, Ghisellini *et al.*1999, Lazzati *et al.*, 1999).

Quantitative calculations of spectral diagnostics of GRB progenitors are hindered by the lack of detailed calculations or data on the evolution and mass loss history in the period of months to years before the outburst. However, it is possible to guess what some of the generic features of such pre-burst environments may be. The purpose of this paper is to consider some very simplified but physically plausible progenitor configurations, and to explore in quantitative detail the range of possible X-ray/UV spectral signatures that can be expected from them in the time scale of hours to days after the outburst.

2. Pre-burst Environments and Computational Method

The task of finding useful progenitor diagnostics is simplified if the pre-burst evolution of the latter leads to a significantly enhanced gas density in the immediate neighborhood of the burst. In the case of a massive progenitor scenario, such as a hypernova or collapsar, it is known that red supergiants and supernova progenitors in general are prone to have strong winds. One would expect such a strong mass loss phase to produce a pre-burst environment which could have the form of a shell, e.g. as inferred in SN 1987a. For instance, a star evolving from a red giant to a blue giant phase might emit first a slower wind, which is later swept up into a shell by a faster wind. In some collapse or compact binary merger scenarios, e.g. of a BH or NS with a White Dwarf or He core left over from a massive companion star, a supernova producing a metal-enriched supernova remnant (SNR) shell might precede the burst. In general the shell would be expected to have dispersed before the burst occurs, but there could be rare cases where this is not the case. Another possible scenario which has been discussed is the delayed collapse of a rotationally stabilized neutron star, which could lead to a burst with a SNR shell around it (Vietri & Stella 1998).

Another geometry characterizing massive progenitor or collapsar models could arise if the giant progenitor is fast-rotating, e.g. due to spin-up from merging with a compact companion.

Then the stellar envelope and the wind would be expected to be least dense inside a funnel-like cavity extending along the orbital-spin axis, with the GRB at the tip of the funnel. However, detailed models for either a funnel-like environment or for a shell resulting from a GRB progenitor are lacking so far. Therefore, our choice of parameters below for these scenarios is purely phenomenological, and guided more by the reported observations than by theoretical considerations.

For the computations, we need to treat in detail the photoionization and recombination of the various ions in the environment material, and to obtain spectra which can be compared to observations we need to consider the time-dependence. The latter is due to the fact that the recombination and ionization has a natural timescale depending on the ambient density, the chemical abundance and the flux received; that the ionizing spectrum from the GRB afterglow varies in time; and that the spectrum observed at a given observer time is made up of light arriving from different regions of the remnant, for which the source time is different. The problem can be simplified if the first timescale is shorter than the latter two, since in this case one may use a steady-state photoionization code. The recombination time is $t_{rec} \sim 10^3 Z^{-2} T_7^{1/2} n_{10}^{-1}$ s for ions of charge Z at the typical temperatures and densities in the reprocessing gas, which is short compared to the timescales $\sim 10^5$ s ~ 1 day considered, so the ionization equilibrium approximation is justified in the examples calculated below. In this paper we exploit this approximation, and make use of the XSTAR code (Kallman & McCray 1982, Kallman & Krolik 1998) to calculate the spectrum. This is a steady state code which, for a given input spectrum, calculates the photoionization of a plasma in a shell at a given distance from the source, as a function of the density and chemical abundances. These position dependent spectra in the source frame, which arise in response to a time-variable input spectrum, are integrated over the remnant to obtain the observer-time dependent spectra that would be actually measured. A restriction on the use of this code is that the effects of comptonization can be included only in a rough manner. This is not a problem if the remnant is Thomson thin (column density $\Sigma \lesssim 2.5 \times 10^{24} \text{cm}^{-2}$), or if the incident continuum is absorbed over a column density smaller than this. Very little if at all is known about the nature and geometry of the remnants, and in what follows we assume situations where the above restriction is either satisfied, or the effects of its violation can be estimated by means of a different Monte Carlo code (Matt *et al.*, 1996) which is not subject to this restriction.

The input spectrum that we assume is typical of simple afterglow models (Mészáros & Rees 1997a, Waxman 1997), with phenomenological parameters chosen to approximate those of the observed afterglow GRB 970508. We take these to be a break luminosity $L_{\epsilon_m} \simeq 3.2 \times 10^{46}$ erg/s/keV with a break energy $\epsilon_m = 1.96$ keV at $t = 10^3$ s, a Band *et al.* 1993 spectrum with energy indices $\alpha = 0.33$, $\beta = -0.75$ and a standard time decay exponent for the peak frequency of $\gamma = -(3/2)\beta$.

3. Shell Models

One type of environment model considered is a shell of gas at some distance from the burst, considered to be essentially stationary over the period of interest for its response to the above time-dependent input spectrum. The shells could be metal-enriched, especially if arising from a supernova explosion before the burst, and possibly also if involving a pre-ejected wind from a massive stellar progenitor (although in the latter, solar abundances are probably likelier). These shells could have a large coverage fraction, and would have a mean density much larger than typical ISM values, especially when blobs and condensations form via instabilities. Guided by the report of an Fe line detection peaking after about one day in GRB 970508 and in GRB 970828 (Piro *et al.*, 1999, Yoshida *et al.* 1998), one is led to consider shell radii $R \gtrsim$ light day. A physical requirement is that the distance $ct\Gamma(t)^2$ reached after one day by the afterglow shock producing the continuum be less than R , with $\Gamma \gtrsim 1$. As an example, we assume that the shock is observed to reach the shell at an inner-radius distance $R \sim 1.5 \times 10^{16}$ cm at $t_s = 1$ day along the L.O.S.. Within the context of simple (adiabatic, impulsive, homogeneous external density) standard afterglow models, this could occur for a deceleration radius $\lesssim R$, requiring a density between the burst and the shell higher than usually considered. A pre-shell density $n \lesssim 10^6 \text{cm}^{-3}$ could do this, involving a total mass $\sim 10^{-2} M_\odot$ much less than in the assumed shell, and a Thomson optical depth $\tau_T \ll 1$. However, in scenarios leading to a shell the conditions might differ substantially from those implied in snapshot fits to simple standard models, e.g. Wijers & Galama 1999, and the error bars in such fits are hard to estimate. A complete model of the physics for both the input continuum and the reprocessing gas would be uncertain, especially in view of the preliminary nature of current X-ray line observations. For this reason, we prefer to consider a phenomenological input spectrum as a quantity given by observations, and treat the environment simply as a test particle gas, choosing its physical parameters in such a manner as to reproduce the current observations.

For computational reasons, the calculations are carried out for thin homogeneous spherical shells of different densities, which can be used to represent thicker inhomogeneous shells with the same mass per unit area and the same density in the filaments or blobs as in a homogeneous thin shell. The shell was assumed to have an Fe abundance either 10 times solar or 10^2 solar (and solar for the other elements), and a hydrogen column density $N_H = 5 \times 10^{23} \text{cm}^{-2}$, with a total mass $M_s \sim 1 M_\odot$. The X-ray/UV spectrum as a function of observer time is shown in Figure 1, for several values of the particle density in the shell. The line spectrum becomes more prominent as the gas cools and recombines. Due to the very high luminosities and hard initial γ -ray spectrum, initially all the Fe is fully ionized, and as it cools the strongest features initially are the Fe K- α and K-edge, which initially appear in absorption and later as recombination *emission* features, the strength of the K-edge feature peaking at later times than the K- α for these luminosities, the K- α line being more prominent and easier to detect for this input continuum luminosity. (For a lower input continuum luminosity with a steeper spectrum, however, the time sequence can reverse and the K-edge can be more prominent than the K- α feature). As the continuum continues to

decrease the Fe K- α line becomes more important, shifting its energy gradually from 6.7 to 6.4 keV as the lower ions become in turn more predominant. At later times the Fe K-edge recombination emission feature begins to emerge in emission as well, whereas at early times it is largely an absorption feature. After the Fe features have become important, with some delay depending on the density and abundance, other features in the 2-3 keV range due to Si and S also become prominent, as well as an O recombination and K- α features at 0.86 and 0.65 keV.

The corresponding X-ray light curves in the 2-10 keV range are shown in Figure 2, as well as the equivalent widths of the Fe K- α feature. The Fe K- α luminosity reaches values $\lesssim 10^{43}$ erg s $^{-1}$ and the EW reaches values of 0.2 to 3.5 keV in emission. The Fe K-edge feature in emission reaches values $\lesssim 0.1$ keV in Figure 2d (not shown), but at early times the K-edge absorption is substantial, as seen in Figure 1. In this example of a full shell the equivalent width (EW) of the Fe K- α in the 6.4-6.7 keV range and the Fe K-edge at ~ 9.28 keV continues to grow as the bulk of the diffuse K-edge recombination and fluorescent K- α photons reach the observer from the rim and the back portions of the shell, in response to the GRB time-dependent continuum. This growth continues until a time $t \sim R/c \sim 5$ days, when the diffuse radiation from the rim of the shell becomes visible. However, by this time the total X-ray flux (continuum plus lines) has decreased significantly (Figure 1) and the S/N is less favorable for detection. Notice that in this calculation the continuum source, i.e. the shock, crosses the shell at 1 day. At this point the observed continuum X-ray luminosity temporarily increases, as the radiation along the L.O.S. is no longer absorbed by the shell, but then it continues to decrease according to the standard afterglow decay law. This temporary brightening would be enhanced, and might be dominated by, the heating of the shell as the shock goes across it; a consistent analysis of the shock heating would require a number of additional assumptions and detailed gas dynamical calculations which are beyond the scope of this paper (see, e.g., Vietri *et al.* 1999 for an analytical estimate). A temporary brightening of the continuum at one day is in fact seen in the observations of GRB 970508 (Piro *et al.*, 1999). The unabsorbed continuum reaching the observer after one day from beyond the shell is also responsible for the gradual re-filling of the absorption troughs seen in Figure 1 at late times.

The effects of a jet-like fireball illuminating a spherical shell is also of interest. An example of the spectral evolution is shown in Figure 3, for a fireball whose continuum radiation is collimated in a jet of opening half-angle $\theta_j = 37$ deg (and other properties the same as for the spherical fireball of Figure 1). In this example the shell was assumed to be spherical, with the same dimensions and properties as in Figure 1. The effect of a jet is that the ring-shaped area of illuminated shell which is visible to the observer increases only up to a time $t_j = (R/c)(1 - \cos \theta_j) \sim 1$ day. After that time, the shell regions at angles larger than θ_j which become visible do not contribute any diffuse radiation, since they are not (and were never) illuminated by the continuum source. This choice of θ_j results therefore in K-edge and K- α equivalent widths which grow until $t_j \sim 1$ day, and decay thereafter (see Figure 4).

4. Scattering Funnel Hypernova Models

A different configuration which may characterize hypernovae involves a funnel geometry. Accurate hypernova line diagnostics will be uncertain due to the absence of quantitative models, extending from minutes to days after the burst, of the gaseous environment in the outer layers and/or winds in such objects. We can, however, get an estimate of what may be expected by using a physically plausible toy model. We take a parabolical funnel as an idealized representation of the centrifugally evacuated funnel along the rotation axis of the collapsing stellar configuration, with the GRB at its tip. In order to produce line features which peak at about one day from such a model, one requires the X-ray continuum to be inside the outer rim of the funnel for at least this long. A simple configuration with these properties is, for example, a wind with a scattering optical depth $\gtrsim 1$ extending out to $R = 1.5 \times 10^{16}$, in which there are two empty (or at any rate much lower density) funnels, inside which the fireball expands. The fireball is assumed to have the same luminosity per solid angle and spectral characteristics as used in the previous two shell models, and the funnel opening half-angle was taken to be 15 deg. For the funnel walls we take a uniform density $n = 10^{10} \text{cm}^{-3}$, and an Fe abundance $x_{Fe} = 10$ or $x_{Fe} = 10^2$; we assume the effective column density within which reprocessing is most effective to be $\Sigma = 10^{24} \text{cm}^{-2}$, the effective amount of reprocessing mass involved being $\sim 0.2 M_{\odot}$. An accurate calculation of the spectrum escaping from a funnel is not straightforward, since a rigorous prescription for treating multiple scatterings and a non-spherical geometry is difficult to implement in a code such as XSTAR. However, it is possible to obtain useful lower and upper limits for the actual equivalent widths, by calculating the widths expected in two limits. A low estimate for the EW is computed by counting only the once-reflected line photons which are directed inside the opening angle of the funnel, and comparing them to the continuum photons (either direct or reflected) which are similarly directed inside the opening angle. The high limit for the EW is calculated using all the once-reflected line photons (whether directed at the opening or not) and comparing them to the directly escaping plus all the reflected continuum. A spectrum as a function of time for the second limit (all) and $x_{Fe} = 10^2$ is shown in Figure 5.

The funnel model was taken to have the same input luminosity per solid angle as the shell models, but the incidence angle is shallower in funnels, and hence the effective heating per unit area is smaller than in shells at the same distance, which favors Fe K- α recombination, hence the Fe K- α luminosity is larger. The upper and lower limits for this hypernova example with $x_{Fe} = 10^2$ (see bottom of figure 5) show that at one day the Fe K- α luminosity is bounded between $2 \times 10^{44} \text{erg s}^{-1}$ and $6 \times 10^{42} \text{erg s}^{-1}$, and the Fe K- α line EW is bounded between 1.2 and ~ 0.1 keV, while the Fe K-edge EW, which is more prominent, is bounded between 2.7 and 0.2 keV. For $x_{Fe} = 10$, these values are lower by a factor ~ 3 (Figure 6).

5. Discussion

We have considered a series of models where the environment of the burst can be represented as a shell of enhanced density at some radial distance from the burst. These shells could be the result of a pre-burst wind phase of a massive progenitor, a hypernova, collapsar or a merger involving a massive companion or its core. Alternatively, they might be supernova remnant (SNR) shells of a rare kind, which originated sufficiently recently that they have not yet dispersed before the burst occurs. Such shells can produce significant Fe K- α and K-edge luminosities and equivalent widths of order \sim keV, provided the density (possibly in the form of blobs) in the shell is large ($10^{10} - 10^{12} \text{cm}^{-3}$), and the coverage fraction is a substantial fraction of 4π . For a mass of Fe in the shell $\sim 2.5 \times 10^{-4} M_{\odot}$ or $2.5 \times 10^{-3} M_{\odot}$ (a total shell mass $1 M_{\odot}$) the Fe K- α equivalent widths after one day can be $E_W \lesssim$ keV, comparable to the values reported by Piro *et al.*, 1999 and Yoshida *et al.* 1998. However, the Fe luminosity is $\lesssim 10^{43} \text{erg s}^{-1}$, which is low by a factor of 5-10. The higher density or more Fe-rich shells also show a drop in the continuum after $t \sim 10^4$ s due to Fe absorption and re-emission, e.g. panels b.c and d of Figure 2, a feature which qualitatively resembles an observed dip in the light curve of GRB 970508 at $\sim 5^4$ s (Piro *et al.*, 1999). We note that winds of $\dot{M} \sim 10^{-4} M_{\odot}/\text{yr}$ with velocities $v_w \sim 100 \text{Km/s}$ varying on timescales $\lesssim 100$ years (characteristic of massive stars) would yield shell enhancements starting at $R \sim 10^{16} \text{cm}$ with mean density $n \gtrsim 10^5 \text{cm}^{-3}$, in which condensations of $n \sim 10^9 - 10^{11} \text{cm}^{-3}$ could form via instabilities. Dense shells may also form as a result of a fast wind following a slower one. The results would be similar whether the shells are homogeneous, or consist of blobs with the same density and a comparable total coverage fraction as a homogeneous shell. (Note that in this model the shell or blobs have a different origin, are further out and are much bulkier and slower than, e.g the metal-enriched blobs possibly accelerated in the relativistically moving burst ejecta itself, e.g. Hailey *et al.* 1999, Mészáros & Rees 1998a).

In this particular model, the Fe K- α EWs reach values $E_W \sim 0.3 - 3 \text{keV}$ at 1 day, and continue to be significant up to a time $\sim R/c \sim 5$ days when the diffuse radiation from the rim of the shell reaches the observer (Figures 1 and 2). However the continued decay of the continuum after 1 day would reduce the S/N ratio, which would make it harder to detect an Fe feature at later times.

We have also explored a different shell scenario, where the Fe features would cut-off abruptly after reaching a peak. This occurs if the continuum is beamed, e.g. it is produced by a collimated fireball jet. In this case (Figures 3 and 4), the diffuse radiation, including the Fe and other spectral features, cuts off after a time $t \sim (R/c)(1 - \cos \theta_j) \sim 1$ day, and for a $\sim 1 M_{\odot}$ shell at $R \sim 10^{16} \text{cm}$ with Fe abundance $10 - 10^2$ times solar the models produce Fe K- α equivalent widths $\lesssim 0.3 - 3 \text{keV}$ (depending on the density) peaking at one day.

Another series of models that we considered address the consequences of a funnel geometry in a spinning massive progenitor (hypernova or collapsar). If the stellar envelope or its wind can be assumed to extend out to radii of light-days with an appreciable density of order

$n \sim 10^9 - 10^{11} \text{cm}^{-3}$ (particularly in winds where the density drops slower than r^{-2} , e.g. as in hour-glass shaped winds such as that of SN 1987a), a wider range of luminosities and equivalent widths is possible after ~ 1 day. In this case, for $x_{Fe} = 10^2$ we obtain an Fe K- α luminosity $L_{Fe} \sim 2 \times 10^{44} \text{erg s}^{-1}$ at $t \sim 1$ day (or a factor 3 lower, for $x_{Fe} = 10$), comparable to the observational results. The equivalent width grows until the continuum source (or afterglow shock) moves beyond the radius where there is a substantial amount of stellar wind material to reprocess it (see Figure 5). After that time, only the decaying shock continuum is detected which is now beyond the wind region, and a fast decaying component from the funnel wall as it cools.

The calculations presented here indicate that a qualitative difference between shell and funnel models is that, whereas shells produce Fe K- α , K-edge and features from other metals predominantly in absorption, and later also partly in emission, the funnel models are dominated by emission features throughout. This is due to the presence of material along the line of sight in the shell models, which is absent in the funnel case.

It is worth noting that in GRB 970508 the energy of the X-ray spectral feature discussed by Piro *et al.*, 1999 agrees with that of a 6.7 keV Fe K- α line at the previously known redshift $z = 0.835$ (Metzger, *et al.*1997), while in GRB 970828 the energy of the X-ray spectral feature reported by Yoshida *et al.*1998 is compatible with an Fe K-edge feature at 9.28 keV in the rest frame, at the recently reported redshift $z = 0.958$ (Djorgovski, *et al.*, 2000).

A general point is that in the case of low mass binary mergers, such as NS-NS or BH-NS, it is harder to see how shells or funnels would have formed and still be present within distances $\gtrsim 10^{15} - 10^{16} \text{cm}$ at the time of the burst. Hence the detection of Fe K-edge and K- α features peaking at ~ 1 day at the strengths discussed here (and as reported by Piro *et al.*, 1999, Yoshida *et al.*1998) would appear to be a significant diagnostic for a massive progenitor. Shells and funnels with dimensions about a light-day are rough examples of extreme geometries which might characterize massive progenitor remnants. However, a clear distinction between various types of massive progenitors (or mergers involving a massive progenitor) would require extensive quantitative calculations in the spirit of, e.g. Fryer, Woosley & Hartmann 1999 and Ruffert & Janka 1999, but considering more specifically the different pre-burst evolution and near-burst environments. What our present calculations are able to indicate is that Fe K- α equivalent widths of $\sim \text{keV}$ can be produced in a variety of plausible progenitor scenarios, but the absolute value of the Fe K- α line flux provides constraints on the combined values of the density, chemical abundance and distance from the burst, as well as the geometry. Our present calculations, which include a number of simplifying assumptions, indicate that Fe-enriched funnel models agrees better than shell models with the currently reported Fe line values. More detailed modeling, as well as more sensitive X-ray spectral line detections, should be able to provide valuable constraints on specific progenitors.

We are grateful to NASA NAG5-2857, NSF PHY94-07194, the Division of Physics, Math & Astronomy, the Astronomy Visitor Program and Merle Kingsley fund at Caltech, the DAAD and

the Royal Society for support. We thank M. Böttcher for pointing out a significant discrepancy, and N. Brandt, G. Chartas, G. Djorgovski, A. Fabian, S. Kulkarni, A. Panaitescu, S. Sigurdsson and A. Young for discussions.

REFERENCES

- Band, D. *et al.*, 1993, ApJ, 413, 281.
- Bisnovatyi-Kogan, G & Timokhin, A, 1997, Astr. Rep. 41, 423
- Bloom, J *et al.*, 1998, A& A Supp., in press (Procs. Rome Conf. on GRB)
- Böttcher, M, *et al.*, 1998, A& A, in press, astro-ph/9809156
- Djorgovski, S.G., *et al.*, 2000, ApJ. subm.
- Fryer, C, Woosley, S & Hartmann, D, 1999, ApJ subm (astro-ph/9904122)
- Ghisellini, G, *et al.*, 1999, ApJ, 517, 168
- Hailey, C, Harrison, F & Mori, K, 1999, ApJ(Letters) in press (astro-ph/9905217)
- Kallman, T & McCray, R, 1982, ApJS, 50, 283
- Kallman, T, and Krolik, J, 1998, XSTAR manual,
<ftp://legacy.gsfc.nasa.gov/software/plasmacodes/xstar>
- Lazzati, D., Ghisellini, G & Campana, S, 1999, MNRAS, 304, L31
- Matt G., Brandt W.N., Fabian A.C., 1996, MNRAS, 280, 823
- Mészáros, P & Rees, M.J., 1997a, ApJ, 476, 232
- Mészáros, P., 1998, Procs. 19th Texas Symp. Relativistic Astrophysics & Cosmology; in Nuclear Phys. B (Procs. Suppl.), Elsevier Science (in press) (astro-ph/9904038)
- Mészáros, P & Rees, M.J., 1998a, ApJ, 502, L105
- Mészáros, P & Rees, M.J., 1998b, MNRAS, 299, L10
- Metzger, M., *et al.*, Nature, 387, 878.
- Owen, A. *et al.* 1998, Astron.&Astrophys. in press (astro-ph/9809356)
- Paczynski, B., 1998, ApJ, 494, L45
- Perna, R. & Loeb, A., 1998, ApJ, 503, L135

Piro, L, *et al.*, 1999, ApJ, 514, L73

Ruffert, M. & Janka, H.-T., 1999, A&A in press (astro-ph/9804132)

Vietri, M & Stella, L, 1998, ApJ, 507, L45

Vietri, M, Perola, C, Piro, L & Stella, L, 1999, MNRAS in press (astro-ph/9906288)

Waxman, E., 1997, ApJ, 489, L33

Wijers, R.A.M.J. & Galama, T., 1999, ApJ, 523, 177.

Yoshida, A, *et al.*, 1998, A& A Supp.,in press (Procs. Rome Conf. on GRB)

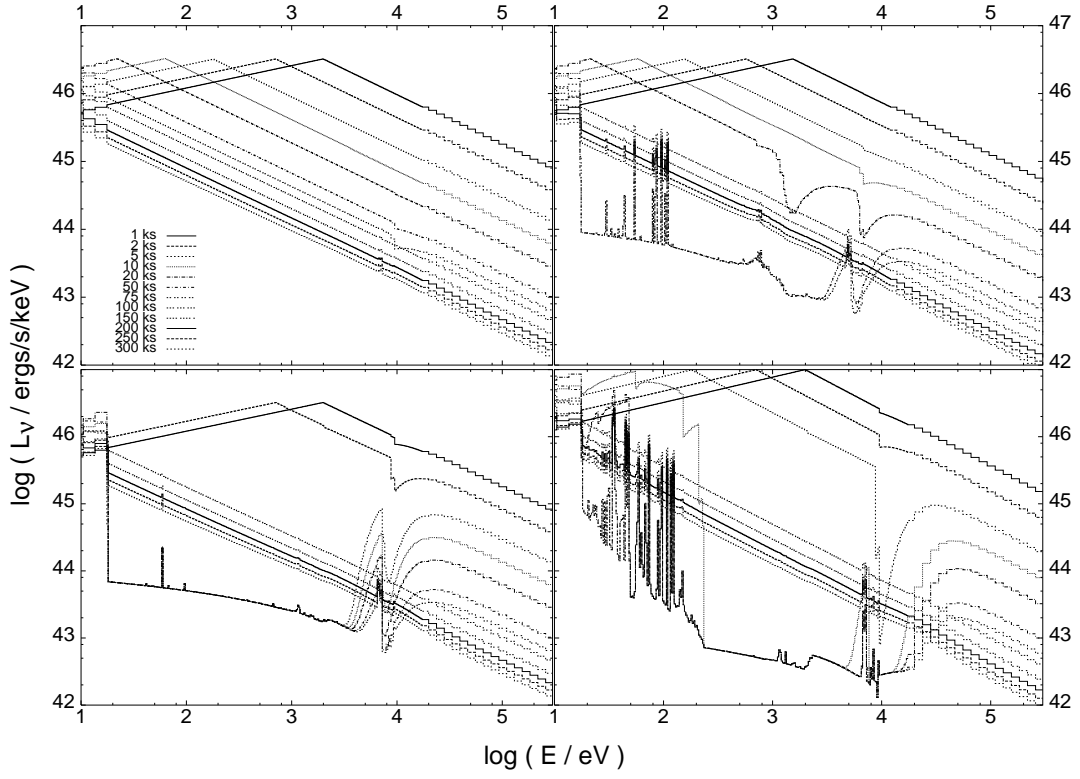


Fig. 1.— Spectrum of a shell model for various observer times (in seconds), with $R = 1.5 \times 10^{16}$ cm, hydrogen column density $\Sigma = 5 \times 10^{23} \text{cm}^{-2}$, for several particle densities n and Fe abundance $x_{Fe} = n_{Fe}/n_{Fe,\odot}$. Top left(a): $n = 10^{10} \text{cm}^{-3}$, $x_{Fe} = 10$; top right(b): $n = 10^{11} \text{cm}^{-3}$, $x_{Fe} = 10$; bottom left(c): $n = 10^{12} \text{cm}^{-3}$, $x_{Fe} = 10$; bottom right(d): $n = 10^{11}$, $x_{Fe} = 10^2$.

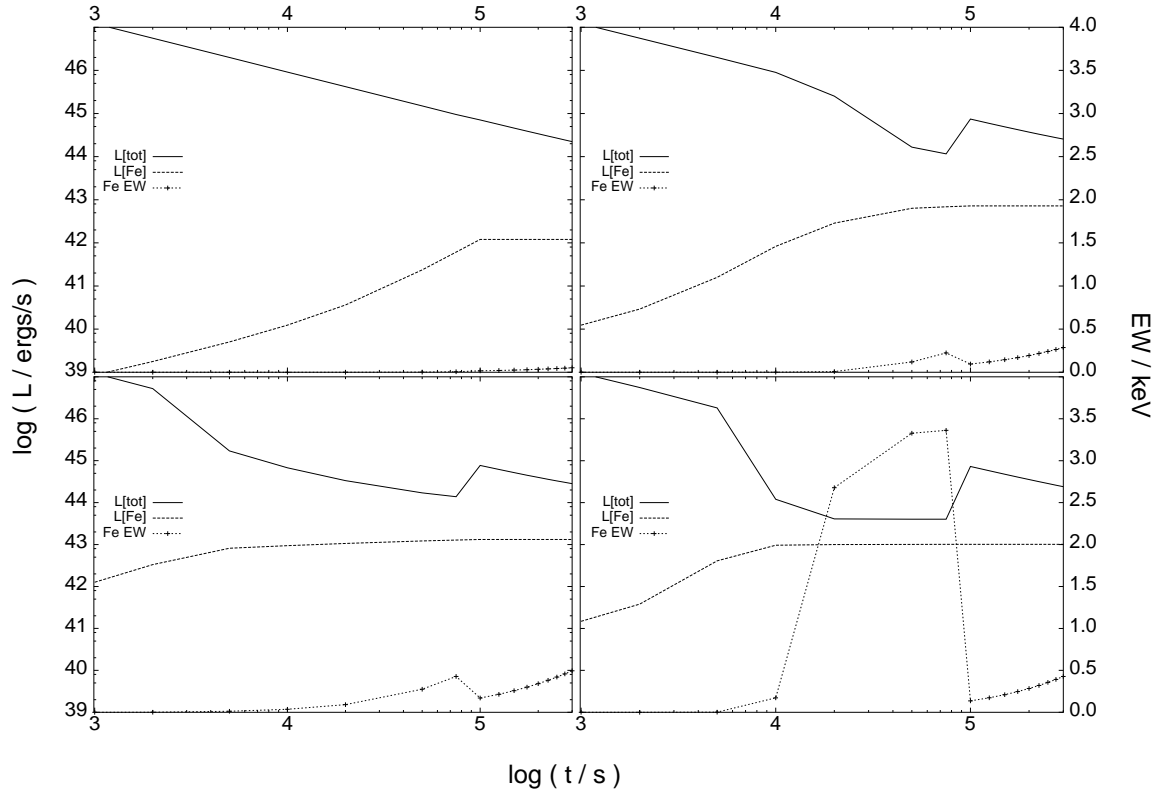


Fig. 2.— Light curves and equivalent width of a shell model, same parameters as in Figure 1. The L_{tot} is the incident plus reprocessed luminosity in the 2-10 keV range, and L_{Fe} is the line luminosity in the Fe K- α range. Top left(a): $n = 10^{10} \text{cm}^{-3}$, $x_{Fe} = 10$; top right(b): $n = 10^{11} \text{cm}^{-3}$, $x_{Fe} = 10$; bottom left(c): $n = 10^{12} \text{cm}^{-3}$, $x_{Fe} = 10$; bottom right(d): $n = 10^{11}$, $x_{Fe} = 10^2$.

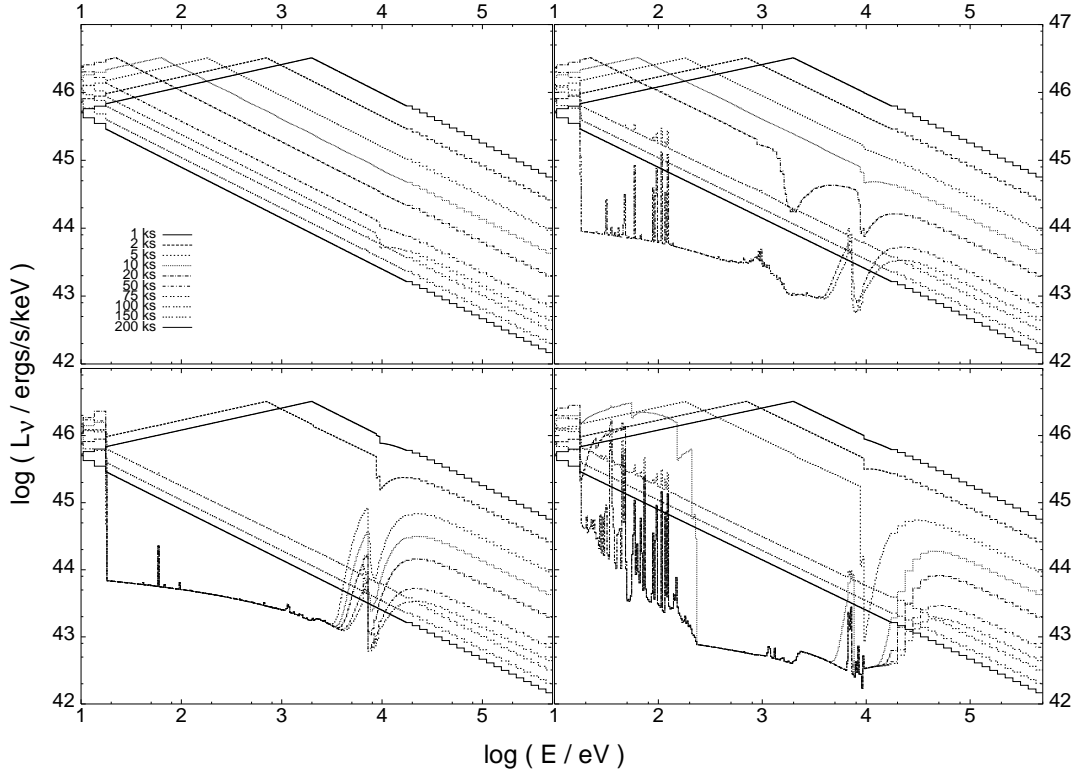


Fig. 3.— Spectrum of a shell model illuminated by a jet-like fireball ($\theta_j = 37$ deg) for various observer times (in seconds), with shell parameters and other fireball properties the same as in Figure 1. Top left(a): $n = 10^{10}\text{cm}^{-3}$, $x_{Fe} = 10$; top right(b): $n = 10^{11}\text{cm}^{-3}$, $x_{Fe} = 10$; bottom left(c): $n = 10^{12}\text{cm}^{-3}$, $x_{Fe} = 10$; bottom right(d): $n = 10^{11}$, $x_{Fe} = 10^2$.

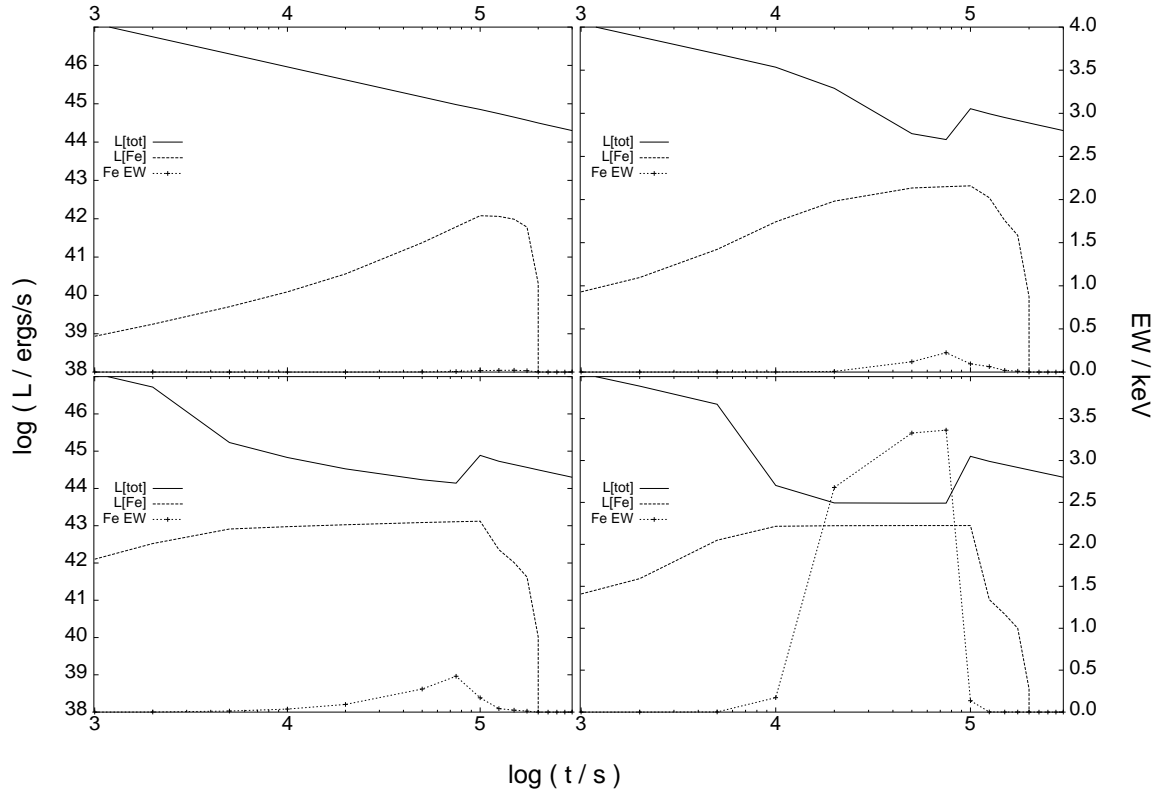


Fig. 4.— Light curves and equivalent width of a shell model illuminated by a jet-like fireball, same parameters as in Figure 3. The L_{tot} is the incident plus reprocessed luminosity in the 2-10 keV range, and L_{Fe} is the line luminosity in the Fe K- α range. Top left(a): $n = 10^{10} \text{cm}^{-3}$, $x_{Fe} = 10$; top right(b): $n = 10^{11} \text{cm}^{-3}$, $x_{Fe} = 10$; bottom left(c): $n = 10^{12} \text{cm}^{-3}$, $x_{Fe} = 10$; bottom right(d): $n = 10^{11}$, $x_{Fe} = 10^2$.

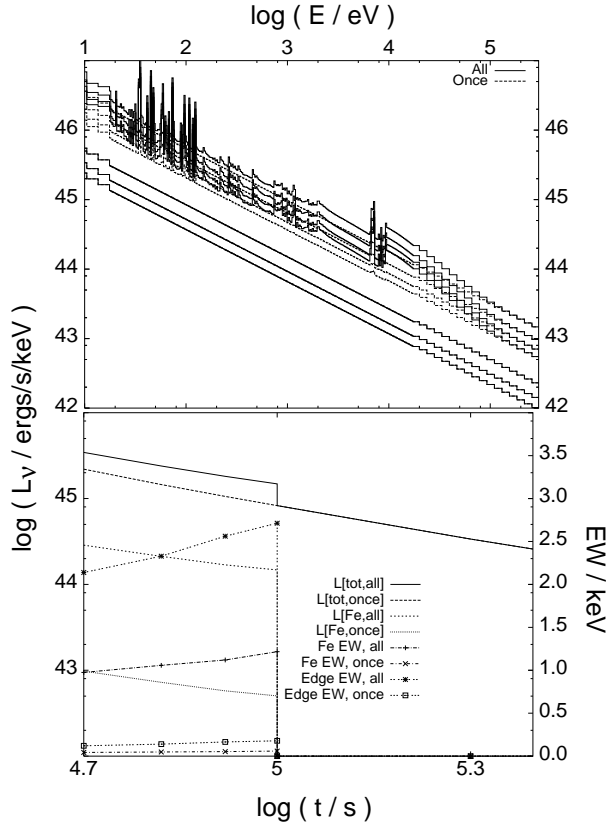


Fig. 5.— *Top*: Spectrum of scattering funnel model with $x_{Fe} = 10^2$ as a function of time (from top to bottom 50, 66, 83, 100, 200 and 300 kseconds). The spectral luminosity is shown in the upper/lower bound approximation (all/once, see text). *Bottom*: Total and Fe light curves and Fe K-edge and K- α equivalent widths for the scattering funnel model as a function of time. The values are calculated for the upper/lower bound approximations (all/once, see text).

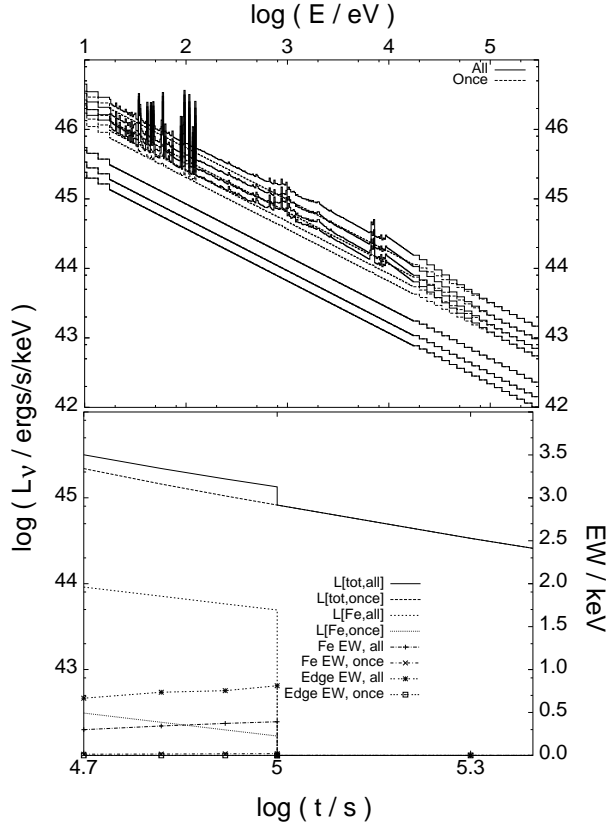


Fig. 6.— *Top*: Spectrum of scattering funnel model with $x_{Fe} = 10$ as a function of time (from top to bottom 50, 66, 83, 100, 200 and 300 kseconds). The spectral luminosity is shown in the upper/lower bound approximation (all/once, see text). *Bottom*: Total and Fe light curves and Fe K-edge and K- α equivalent widths for the scattering funnel model as a function of time. The values are calculated for the upper/lower bound approximations (all/once, see text).